Electronic Supplementary Material (ESI) for Green Chemistry.
This journal is © The Royal Society of Chemistry 2018

Supplementary Information

Ag photoionization–induced single–pass assembly of Ag_2S nanodots in flowing thiol droplets

*Bijay Kumar Poudel,[a] Kyung–Oh Doh[*b] and Jeong Hoon Byeon[a*]*

Dr. Bijay Kumar Poudel and Dr. Jeong Hoon Byeon

[a]School of Mechanical Engineering, Yeungnam University, Gyeongsan 38541, Republic of Korea

Dr. Kyung–Oh Doh

[b]Department of Physiology, Yeungnam University, Daegu 42415, Republic of Korea

[*]Corresponding authors: postjb@yu.ac.kr and kodoh@ynu.ac.kr

METHODS

- ***Assembly of Ag_2S nanodots***

As shown in **Fig. S1**, Ag nanoagglomerates were produced via a laboratory-made spark ablation reactor (volume, 42.8 cm^3) comprising two Ag rods (AG-402561, Nilaco, Japan) and were continuously carried by nitrogen gas (99.999% purity; 3 L min^{-1}) to a collison atomizer to be injected into a solution containing 1-hexanethiol (0.2 v/v% in ethanol) for the photoinduced conversion of Ag nanoagglomerates. Droplets containing Ag nanoagglomerates and 1-hexanethiol were exposed for 6.4 s to 185-nm wavelength photoirradiation (E = 6.2 eV, I = 0.14 J m^{-2} s^{-1}; 3SC-9-A0, UVP, UK) to eject electrons from primary Ag particles (work function, 4.5 eV) in the nanoagglomerates. The surfaces of positively charged Ag were electrostatically reacted with negatively charged thiol groups, resulting in the formation of Ag_2S nanodots (**Fig. 1**a). The solvent was extracted from the droplets as they passed through a denuder containing pelletized activated carbons and silica gel. The negatively charged nanodots due to surface thiolates were subsequently collected on a polished aluminum rod under an electric field (+2.7 kV cm^{-1}) via electrostatic attraction. The collecting rod was then immersed in PBS under ultrasonication (40 kHz) for 5 min to release the nanodots from the rod, forming a nanodot dispersion that was used in bioassays.

- ***Assembly of Ag_2S@TiO_2 nanocomposites***

The assembled Ag_2S nanodots were collided with TiO_2 nanoparticles under an alternating electric field (2.5 kV cm^{-1}, 1 kHz) in a co-current flow configuration. To synthesize TiO_2 nanoparticles in gas stream, the vaporized $TiCl_4$ precursor (208566, Sigma-Aldrich, USA) was fed into a hydrogen flame (hydrogen-1.2 L min^{-1}, air 6.0 L min^{-1}) via bubbling air (0.3 L min^{-1}) passing around the four capillaries inside a quartz burner under ultrasound (20 kHz, 300 W) irradiation near the top-side of the flame. The synthesized TiO_2 particles passed through the tube furnace containing silica gel and activated carbon pellets to remove gaseous residues, and this flow with positive ions (from a carbon brush ionizer) was

injected into Ag_2S nanodot flow for electrostatic agglomeration between TiO_2 and Ag_2S to form $Ag_2S@TiO_2$ nanocomposites. The nanocomposites were thermophoretically deposited on an ultrasonically cleaned fluorine-doped tin oxide (FTO) substrate placed on a Peltier cooler plate (-4°C).

- ***Characterizations***

1) Size distribution in aerosol and aqueous states

The size distribution of fabricated AgNPs (i.e., nanoagglomerates), and thiol and AgNP@thiol droplets were determined using SMPS (3936, TSI, USA) to confirm quantitative interaction between the Ag nanoagglomerates and thiol droplets. The flow rates of sampling and sheathing for SMPS measurements were 0.1 and 1.0 L min^{-1}, respectively, and the scan time was 135 s. DLS (Nano-ZS, Malvern Instruments, UK) was employed to measure the size distribution of Ag nanoagglomerates and Ag_2S nanodots dispersed in PBS.

2) Morphological and crystalline analyses

The fabricated nanodots were directly collected on a carbon-coated copper grid (Tedpella, USA) via TEM grid filtration (Ineris, France) in a gaseous single-pass configuration with no pre- and post-treatments. The Ag nanoagglomerates were also collected on another grid for comparison purposes. The grid was transferred to a holder for TEM analyses (CM-100, FEI/Philips, USA) at increasing voltages in the range of 46-180 kV. The crystalline conversion from Ag into Ag_2S was also examined through XRD (D/MAX-2500, Rigaku, Japan) measurements. The gas-phase fabricated Ag and Ag_2S were directly deposited on glass discs, and these discs were placed on the XRD equipment.

3) Surface chemistry and light absorption

The surface chemistry of nanodots was evaluated using FTIR (iS-10, Thermo Electron, USA) in absorbance mode (1300-3300 cm^{-1}) after nanodot deposition onto a polytetrafluoroethylene substrate (11807-47-N, Sartorius, Germany). Difference in the surface structure between the Ag nanoagglomerates and Ag_2S nanodots were confirmed using XPS (Axis-HIS, Kratos Analytical, Japan). The light absorption spectra of Ag nanoagglomerates and Ag_2S nanodots dispersed in PBS were measured using UV-vis spectroscopy (T60, PG Instruments, UK). The PL spectrum and decay of Ag_2S

nanodots were detected using a fluorescence spectrophotometer (Fluoromax-4, HORIBA, Japan).

4) Photocurrent generation

Photocurrent measurements were performed using electrochemical workstation (CHI660B, CH Instruments, Inc., USA). The workstation was comprised of three electrodes, a single-compartment quartz cell which was filled with 0.1 M Na_2S electrolyte (20 mL) and a potentiostat. A platinum black sheet was used as a counter electrode with Ag/AgCl/KCl as a reference electrode. A thin film of the sample (25 mm × 17 mm) was employed as a working electrode. A 300 W Xe arc lamp (Newport, USA) equipped with an AM 1.5 cutoff filter was used as exciting light source for light irradiation (100 mW cm^{-2}).

5) IPCE measurement

Directly deposited Ag_2S@TiO_2 nanocomposites were doctor-bladed (10 μm thick) onto an FTO substrate. After sintering at 450°C for 1 h, the substrate was immersed in 0.3 mM N719 dye in acetonitrile/tert-butyl alcohol (1:1, v/v) at room temperature for 15 h, followed by rinsing with ethanol and drying in air to remove the non-adsorbed dyes. Platinum counter electrodes were prepared by sputtering method at 20 mA for 60 s at a power 150 W. The dye-adsorbed substrate and counter electrode were stacked and sealed with 60 μm thermal-plastic parafilm spacers at 100°C. Iodide-based liquid electrolyte was injected into the sandwiched cells through the pre-punched holes in the platinum electrode. Lastly, it was sealed by parafilm and cover glass at elevated temperature. IPCE of the cells was measured using a solar cell IPCE measurement system (Solar Cell Scan 100, Zolix, China).

- ***Biological assays***

1) Cytotoxicity

Cytotoxicity measurements for Ag nanoagglomerates and Ag_2S nanodots were measured in MCF-7 and HeLa cells via MTT assay after 48-h incubation. Briefly, 1×10^4 cells per well were plated into 96-well microtiter plates (Becton Dickinson Labware, USA) and incubated for 12 h for cell attachment. After 48 h, the cells were washed, and 100-μL MTT solution (1.25 mg mL^{-1}) was added into each well. During a

4-h incubation in the dark, live cells produced violet-colored formazan crystals as a product of MTT metabolism. The crystals were dissolved in 100-μL DMSO, and the absorbance was measured at 570 nm using a microplate reader (Multiskan EX, Thermo Scientific, USA). Cell viability was calculated as $A_{sample}/A_{control} \times 100\%$, where A is the absorbance at 570 nm.

2) Oxidative stress

Cell-mediated ROS, which is the marker of intracellular oxidative stress, was detected using 2',7'-dichlorodihydrofluorescein diacetate (DCFH-DA). A549 cells were incubated with the particles for 24 h. After washing with PBS, the cells were cultured in serum-free DMEM containing 10 μM DCFH-DA for 30 min at 37°C. The cells were then washed with PBS, harvested by enzymatic release with 0.25% trypsin, washed once again with PBS, and re-suspended in 500 μL PBS. DCFH-DA was hydrolyzed and oxidized to fluorescent 2',7'-dichlorofluorescein (DCF) in the presence of ROS. DCF formed in the PBS-suspended cells was excited with a 488-nm argon ion laser in a flow cytometry system, and the emission was recorded at 525 nm.

3) Hemolysis assay

Red blood cells were incubated with Ag and Ag_2S samples (10-100 μg mL^{-1}) at 37°C for 1 h followed by centrifugation (3000 ×g, 10 min). The percentage of hemolysis was calculated by measuring UV-vis spectra of the supernatant. The negative control was untreated supernatant while positive control was red supernatant caused by 100% hemolysis caused by addition of 1% Triton X-100.

4) Fluorescent microscopy

1×10^5 cells per well were seeded in 6 well culture plates one day before nanodot treatment, and media were changed with media having nanodots. After 24 h incubation with nanodots, the cells were washed three times with PBS. Then the cells were fixed with 4% paraformaldehyde for 10 min and washed three times with PBS. Cellular actin was stained with phallodin (CytoPainter Phalloidin-iFlour 594, Abcam, UK) in PBS for 30 min after 1 mL of 0.1% Triton-X 100 treatment for 5 min. After washing three times with PBS, cells were observed using a fluorescent microscope (BX51, Olympus, Japan).

FIG. S1

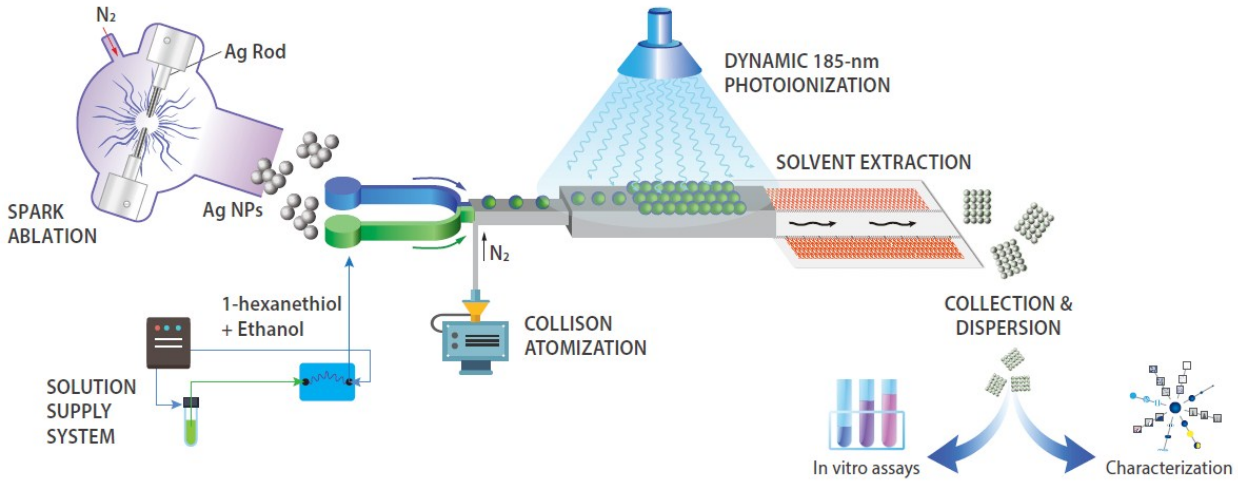

Conversion of Ag nanoagglomerates to Ag_2S nanodots through photoinduced single-pass process in gas stream under 185-nm UV irradiation. AgNPs (i.e., Ag nanoagglomerates) were first prepared via spark ablation between two identical Ag rods, and the nanoagglomerates were then introduced into the 1-hexanethiol solution before the orifice of a collison atomizer. The nanoagglomerates and thiol droplets were sprayed out to form hybrid droplets, which were subsequently exposed to 185-nm UV (6.2 eV) for photoionization of Ag nanoagglomerates (4.5 eV) and subsequent electrostatic reaction with 1-hexanethiol in the irradiation chamber. The reacted droplets then passed through a denuder packed with pelletized activated carbons and silica gels to extract solvent from the droplets, resulting in the formation of Ag_2S nanodots. The nanodots were electrostatically collected (+ field) in an aerosol state and dispersed in PBS for *in vitro* bioassays.

FIG. S2

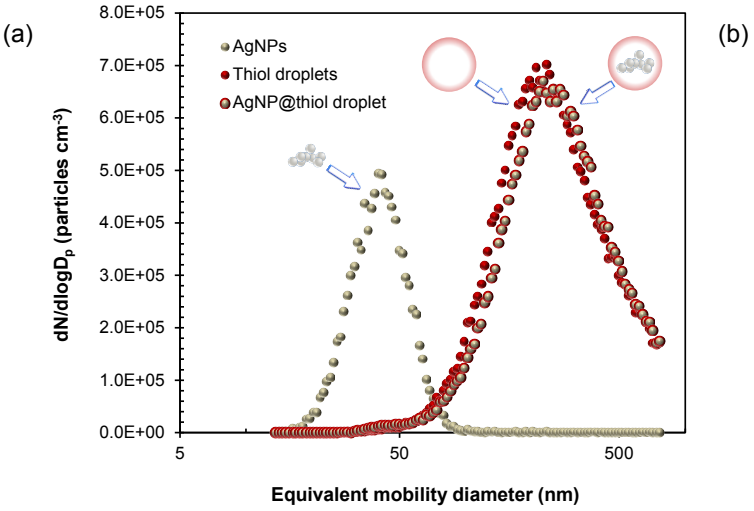

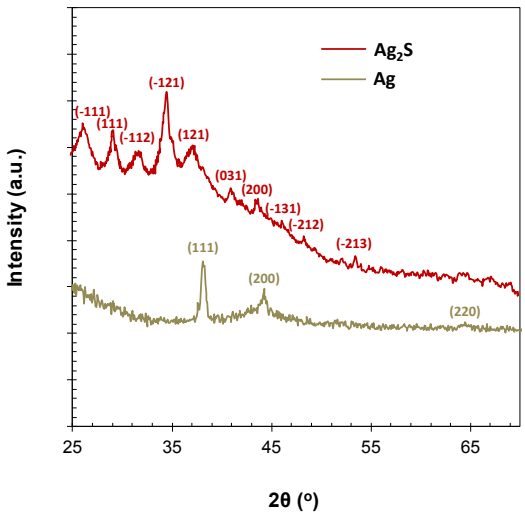

	AgNPs	Thiol droplets	AgNP@thiol droplet
GMD	40.2	239.8	253.6
GSD	1.37	1.73	1.72
TNC	1.5E+05	4.1E+05	3.9E+05

1-hexanethiol in EtOH: 0.2 v/v%

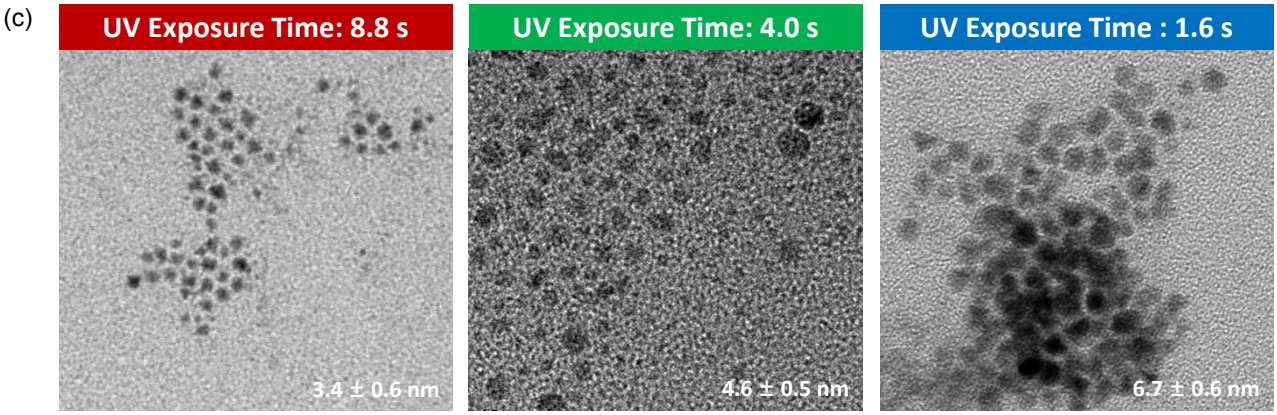

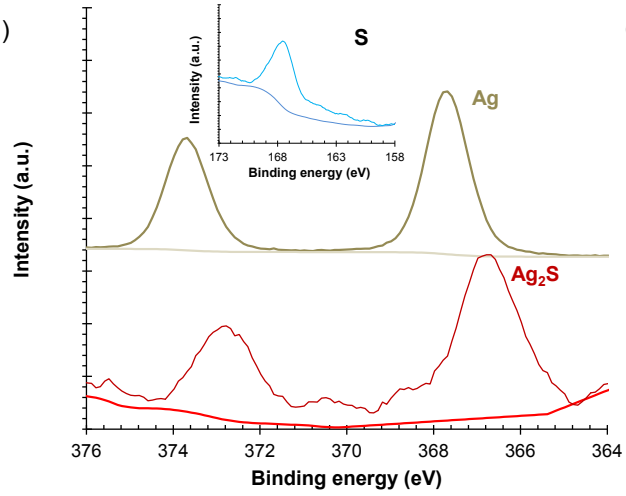

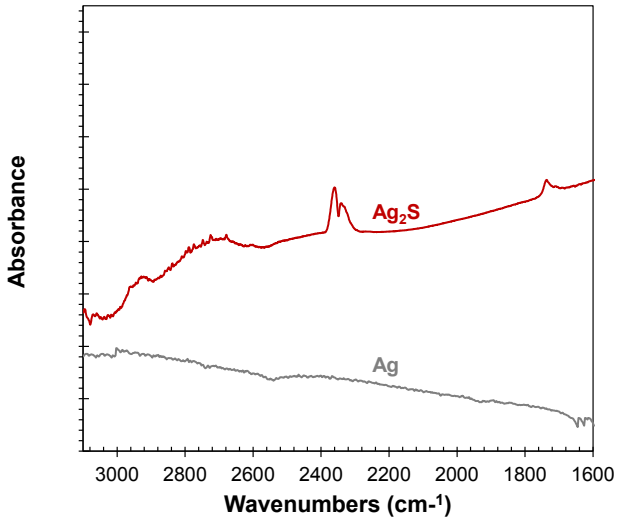

(a) Size distribution of Ag nanoagglomerates (AgNPs), thiol droplets (diluted by ethanol), and hybrid droplets (AgNP@thiol droplet) under 185-nm photoirradiation before solvent extraction via diffusion dryer measured by SMPS. Summaries [geometric mean diameter (GMD), geometric standard deviation (GSD), and total number concentration (TNC)] of the distributions are also displayed. (b) XRD patterns of Ag nanoagglomerates and Ag_2S nanodots. The face-centered-cubic structure of Ag was converted into Ag_2S crystals with (-121) and other planes, which further demonstrates the conversion from Ag into Ag_2S via photoinduced single-pass process in gas stream under 185-nm UV irradiation. (c) TEM images of Ag_2S nanodots from different UV exposure times for the single-pass process. The different status of photoionization of Ag induced variations in size and alignment of Ag_2S. (d) XPS Ag spectra before (Ag nanoagglomerates) and after (Ag_2S nanodots) the photoinduced reaction. The spectrum of Ag_2S shows asymmetric peaks at binding energies of 374 eV and 368 eV respectively corresponding to Ag $3d_{3/2}$ and Ag $3d_{5/2}$ electronic configuration with a splitting of 6 eV. S spectrum (167 eV binding energy) for Ag_2S nanodots is shown as inset. (e) FTIR spectra of Ag nanoagglomerates and Ag_2S nanodots.

FIG. S3

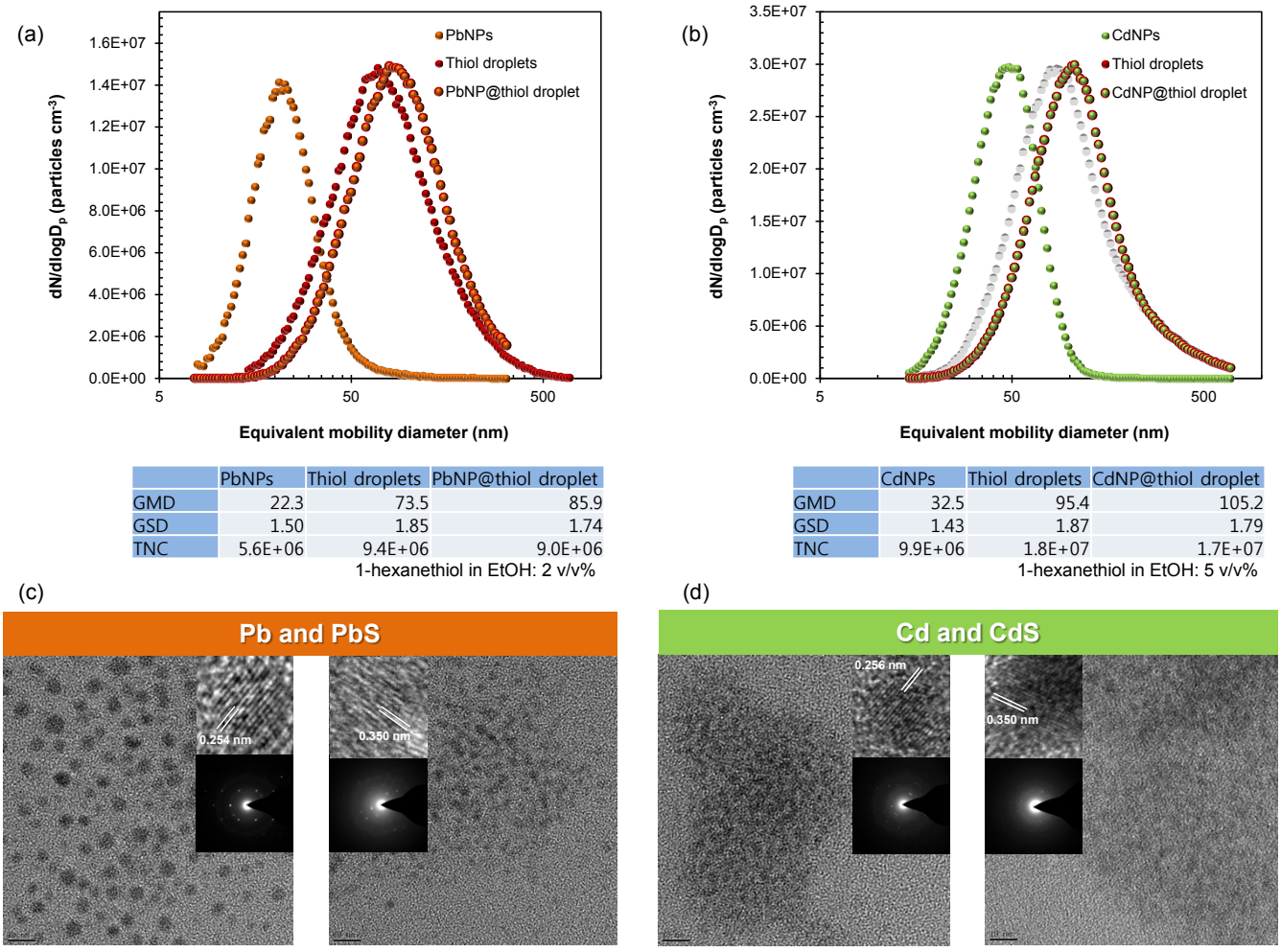

	PbNPs	Thiol droplets	PbNP@thiol droplet
GMD	22.3	73.5	85.9
GSD	1.50	1.85	1.74
TNC	5.6E+06	9.4E+06	9.0E+06

1-hexanethiol in EtOH: 2 v/v%

	CdNPs	Thiol droplets	CdNP@thiol droplet
GMD	32.5	95.4	105.2
GSD	1.43	1.87	1.79
TNC	9.9E+06	1.8E+07	1.7E+07

1-hexanethiol in EtOH: 5 v/v%

Size distributions and morphologies. (a, b) Size distribution of NPs (Pb and Cd), thiol droplets, and NPs (Pb and Cd)@thiol droplets measured by SMPS. Summaries (GMD, GSD, and TNC) of the distributions are also displayed. (c, d) Low- and high-magnification TEM images before (Pb and Cd) and after (PbS and CdS) the photoinduced reaction. *d*-spacing values and selected area electron diffraction patterns for each TEM image are noted as insets. TEM images of primary Pb particles show lattice fringes of 0.254 nm spacing attributed to (020) planes. PbS nanodots exhibited a lattice distance of 0.35 nm corresponding to (111) plane of cubic PbS structure. Analogous data for Cd and CdS particles are 0.25 nm [(0001) plane of hexagonal Cd] and 0.35 nm [(111) plane of cubic CdS], respectively.

FIG. S4

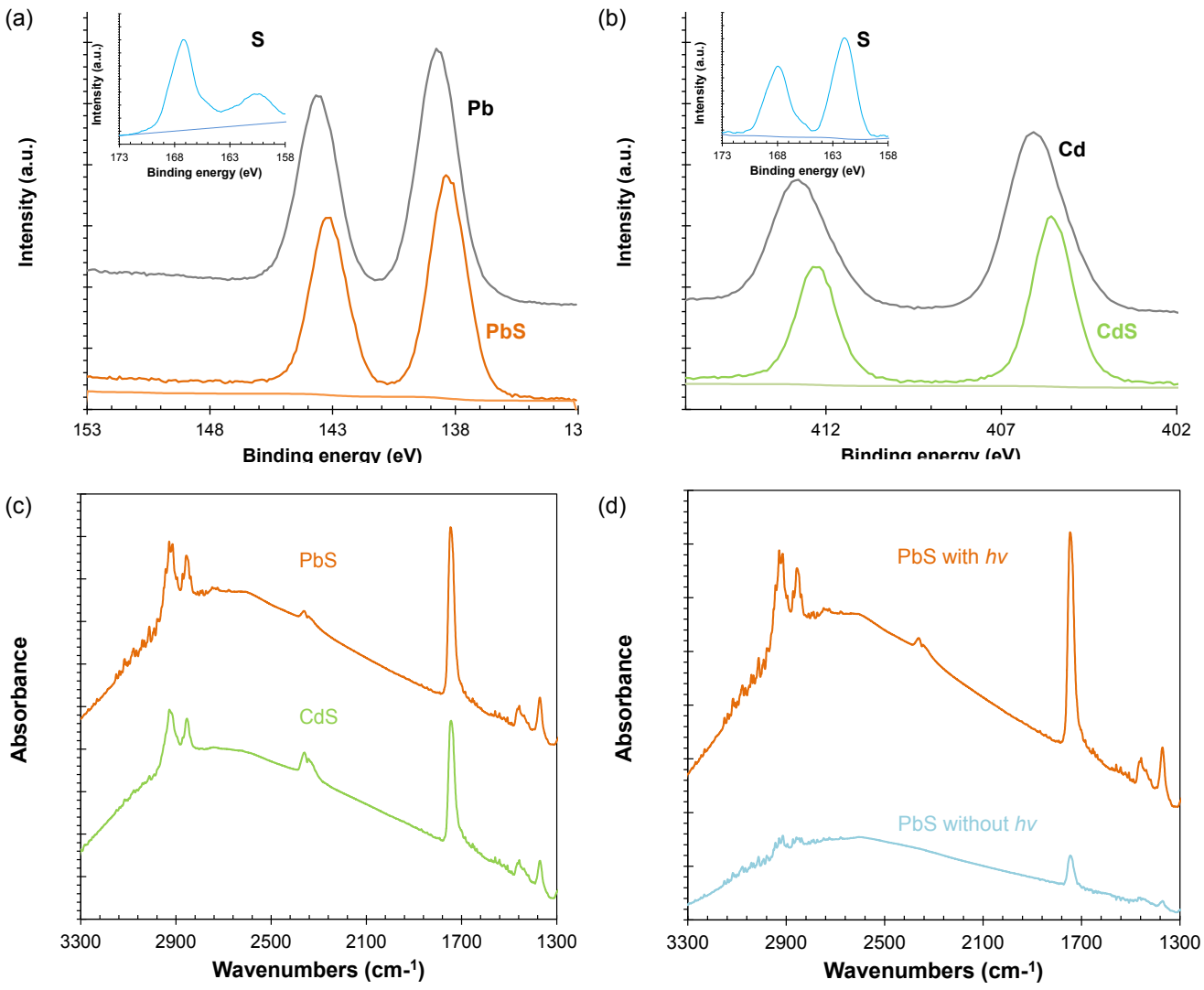

Surface chemistry of PbS and CdS samples. (a, b) XPS spectra before (Pb and Cd) and after (PbS and S; CdS and S) the photoinduced reaction. The Pb 4*f* core displays two characteristic sharp peaks of Pb $4f_{5/2}$ and Pb $4f_{7/2}$ at the binding energies of 143 eV and 138 eV, respectively, with spin orbit separation of 5 eV. Peaks at 167 eV and 161 eV of the inset correspond to S 2p doublet. The peaks for Cd $3d_{3/2}$ and Cd $3d_{5/2}$ of CdS nanodots occurred at the binding energies of 412 eV and 405 eV, respectively. The spin-orbit split of S 2p doublets at low binding energy (~161 eV) can be assigned to bulk and surface S atoms attached to metal atoms, while those at high binding energy (~163 eV) might be attributed to surface S atoms from hexanethiol. (c) FTIR spectra of PbS and CdS, and (d) PbS with and without UV-185 nm

irradiation. The spectra of PbS and CdS display two intense bands at 2920 cm^{-1} and 2880 cm^{-1} are corresponded to the ν(CH) vibrations of CH_2 groups of hexanethiol. Intense signal was also observed at ~1720 cm^{-1}, which can be attributed to the antisymmetric ν(C=O) stretching vibration.

FIG. S5

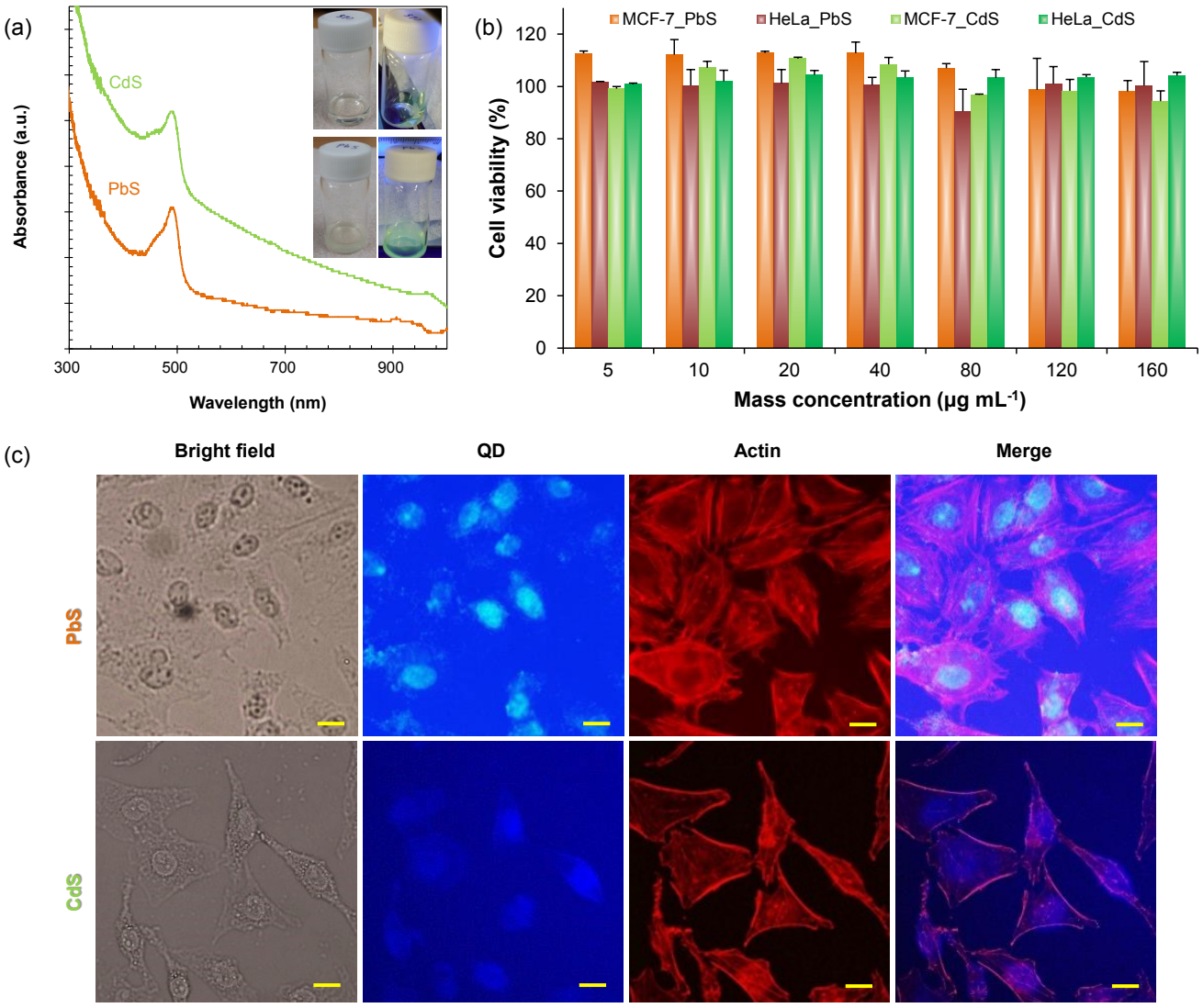

Optical, cytotoxic, and fluorescent properties of PbS and CdS samples. (a) UV-vis spectra with fluorescent images (dispersion under 365-nm UV irradiation). (b) Viability measurements of MCF-7 and HeLa cells treated PbS and CdS as function of mass concentration (5-160 μg mL^{-1}). The studies in MCF-7 and HeLa cells were performed by MTT assay. The cell viability after 24 h incubation remained above 85% in both cells, suggesting that PbS and CdS nanodots warrant bioimaging studies. (c) Fluorescence images of HeLa cell incubated with PbS and CdS samples for 24 h. The mass concentration of samples was 50 mg mL^{-1}. The actin of cells were stained with alexa 594 labeled phallodin to show the shape of cells. Scale bars = 20 μm.

FIG. S6

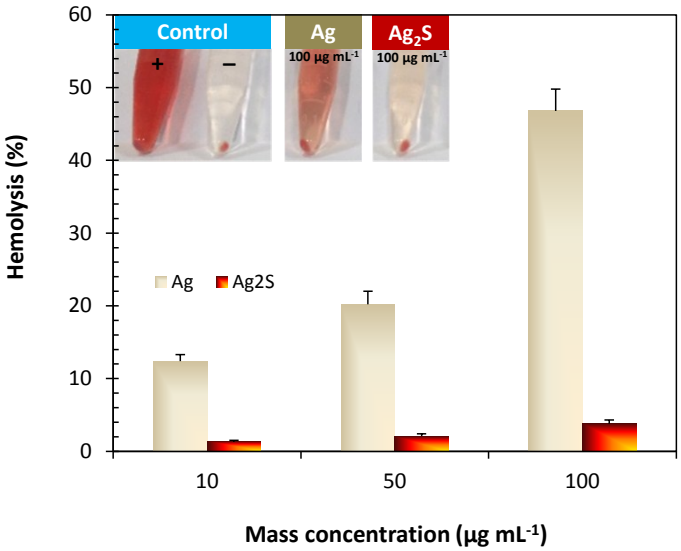

Hemolysis results of Ag and Ag_2S samples. Insets show images for Ag and Ag_2S at 100 µg mL^{-1} concentration, including positive and negative controls.

FIG. S7

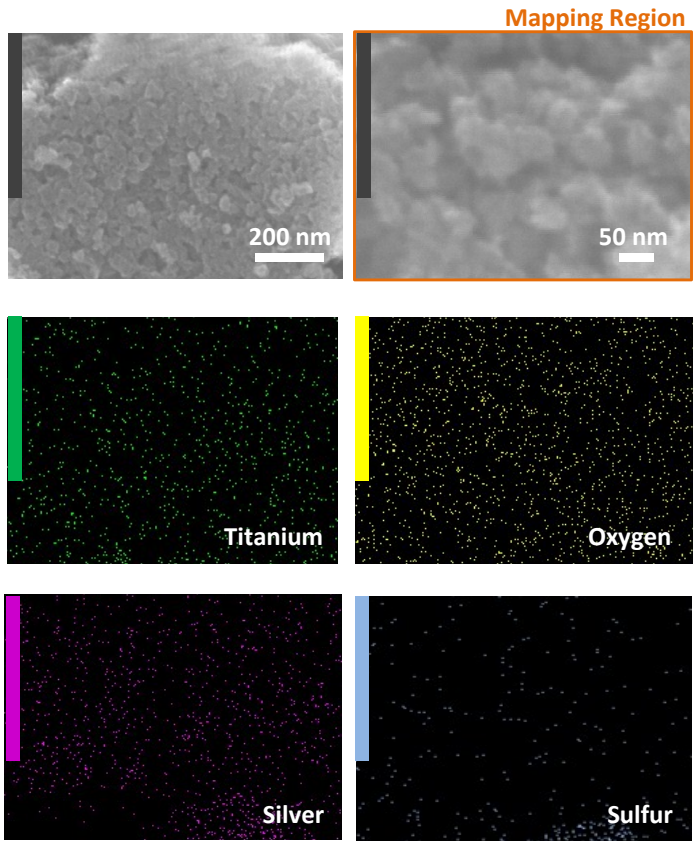

Element	Atomic Percentage (%)
Titanium	23.7
Oxygen	47.5
Silver	19.2
Sulfur	9.6

Low- and high-magnification SEM images and EDX maps of $Ag_2S@TiO_2$ film. Inset table (bottom) shows atomic fractions of Ti, O, Ag, and S elements within the film.

FIG. S8

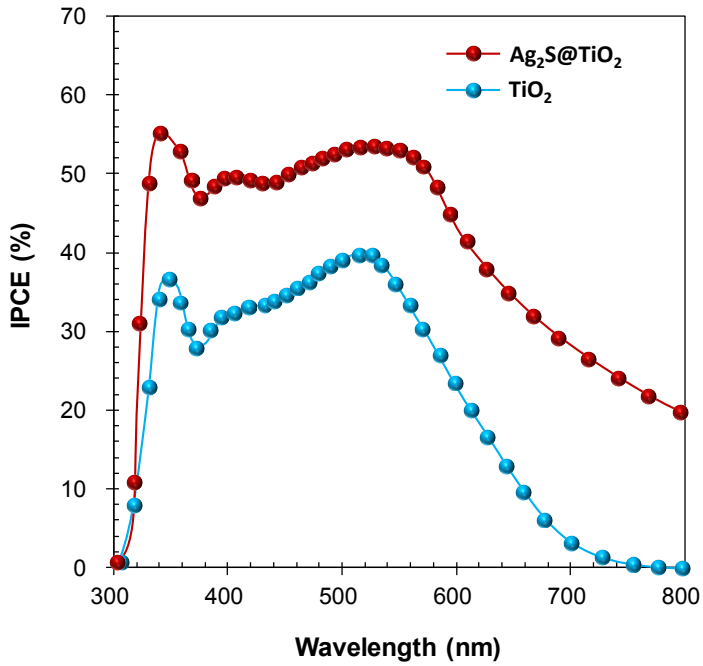

IPCE (%) of $Ag_2S@TiO_2$ solar cells. Flame-synthesized TiO_2 nanoparticle flow was combined to Ag_2S nanodot flow in the presence of alternating electric field in a co-current flow configuration for electrostatic agglomeration between Ag_2S and TiO_2 before they were deposited on an FTO substrate.